



# AMERICAN METEOROLOGICAL SOCIETY

*Journal of Climate*

## **EARLY ONLINE RELEASE**

This is a preliminary PDF of the author-produced manuscript that has been peer-reviewed and accepted for publication. Since it is being posted so soon after acceptance, it has not yet been copyedited, formatted, or processed by AMS Publications. This preliminary version of the manuscript may be downloaded, distributed, and cited, but please be aware that there will be visual differences and possibly some content differences between this version and the final published version.

The DOI for this manuscript is doi: 10.1175/JCLI-D-17-0392.1

The final published version of this manuscript will replace the preliminary version at the above DOI once it is available.

If you would like to cite this EOR in a separate work, please use the following full citation:

Vigaud, N., M. Ting, D. Lee, A. Barnston, and Y. Kushnir, 2018: Multi-scale variability in North American summer maximum temperatures and modulations from the North Atlantic simulated by an AGCM. *J. Climate*. doi:10.1175/JCLI-D-17-0392.1, in press.



1 **Multi-scale variability in North American summer maximum temperatures**  
2 **and modulations from the North Atlantic simulated by an AGCM**

3 Nicolas Vigaud\*

4 *International Research Institute for Climate and Society, Earth Institute at Columbia University,*  
5 *Palisades, New York, USA.*

6 M. Ting, D.-E. Lee

7 *Lamont-Doherty Earth Observatory, Earth Institute at Columbia University, Palisades, New*  
8 *York, USA.*

9 A.G. Barnston

10 *International Research Institute for Climate and Society, IRI, Earth Institute at Columbia*  
11 *University, Palisades, New York, USA.*

12 and Y. Kushnir

13 *Lamont-Doherty Earth Observatory, Earth Institute at Columbia University, Palisades, New*  
14 *York, USA.*

15 \* *Corresponding author address:* International Research Institute for Climate and Society, IRI, Earth

16 Institute at Columbia University, 61 Rte 9W, Palisades, NY 10964, USA

17 E-mail: nicolas.vigaud@gmail.com

## ABSTRACT

18 Six recurrent thermal regimes are identified over continental North Amer-  
19 ica from June to September through a *k* – *means* clustering applied to daily  
20 maximum temperature simulated by ECHAM5 forced by historical SSTs for  
21 1930-2013 and validated using NCEP-DOE II reanalysis over the 1980-2009  
22 period. Four regimes are related to a synoptic wave pattern propagating  
23 eastwards in the midlatitudes with embedded ridging anomalies that trans-  
24 late into maximum warming transiting along. Two other regimes, associated  
25 with broad continental warming and above average temperatures in the north-  
26 east US, respectively, are characterized by ridging anomalies over America,  
27 Europe and Asia that suggest correlated heat waves occurrences in these re-  
28 gions. Their frequencies are both mainly related to La Niña and warm con-  
29 ditions in the North Atlantic. Removing all variability beyond the seasonal  
30 cycle in the North Atlantic in ECHAM5 leads to a significant drop in the  
31 occurrences of the regime associated with warming in the northeast US. Su-  
32 perimposing positive (negative) anomalies mimicking the AMV in the North  
33 Atlantic translates into more (less) warming over the US across all regimes,  
34 and does alter regime frequencies but less significantly. Regime frequency  
35 changes are thus primarily controlled by Atlantic SST variability on all time-  
36 scales beyond the seasonal cycle, rather than mean SST changes, whereas the  
37 intensity of temperature anomalies are impacted by AMV SST forcing, due to  
38 upper-tropospheric warming and enhanced stability suppressing rising motion  
39 during positive phase of the AMV.

## 40 **1. Introduction**

41 Extreme heat episodes are considered to be one of the most deadly weather-related disasters with  
42 dramatic impacts on health, agriculture and the economy across the US (Peterson et al. 2013). Their  
43 increasing severity in the recent decades, together with more frequent occurrences in future pro-  
44 jections over the US and Europe (Meehl and Tebaldi 2004), have heightened concerns. In addition,  
45 a significant increase in the percentage of global land areas subject to extreme temperatures has  
46 been observed from both historical records and coupled models from CMIP5 (Coumou and Robin-  
47 son 2013), further stressing the need for skillful predictions. While at global scale anthropogenic  
48 forcing has been related to trends in extreme heat events (Christidis et al. 2005; Field et al. 2012;  
49 Peterson et al. 2013), its effects are not strong enough to offset the influence of natural variability  
50 on continental scales (Brown et al. 2008). Hence, there is a need to improve our knowledge of  
51 the influence large-scale recurring patterns of variability on heat waves and underlying physical  
52 processes in order to improve projection scenarios and understand better the role anthropogenic  
53 forcing may play in the future. Thus, the goal of this study is to examine recurrent thermal regimes  
54 conducive to warming over North America in summer and their relationship to large-scale patterns  
55 of climate variability, in particular the Atlantic Multi-decadal Variability (AMV) using historical  
56 and forced multidecadal Atmospheric General Circulation Model (AGCM) simulations.

57 Among the known physical drivers, previous case studies emphasized the substantial con-  
58 trols exerted by quasi-stationary Rossby waves on the development of quasi-permanent ridges  
59 or blocking-highs prevailing over North America during heat wave events (Lyon and Dole 1995;  
60 Schubert et al. 2011). Recently, Teng et al. (2013) have identified a wave number-5 pattern arising  
61 mainly from internal atmospheric dynamics and generally found to precede heat waves by 15-20  
62 days. The Madden-Julian Oscillation or MJO (Madden and Julian 1971) modulates tropical heat-

ing and is also a potential trigger for the development of extreme heat events over North America (Lau and Waliser 2011). In addition, a circulation pattern of semistationary ridging anomalies at 500 hPa conducive to observed heat waves over North America and Europe and intensified under increasing greenhouse gases concentrations (Meehl and Tebaldi 2004), is projected to increase heat waves intensity, frequency and persistence by the end of the 21<sup>st</sup> century with an upward trend that should even become apparent in the early decades (Lau and Nath 2012).

At local scale, a soil moisture deficit from the previous season leading to less evapotranspiration but higher sensible heat flux to the atmosphere, can create a positive soil moisture-rainfall feedback (Betts and Ball 1998; Eltahir 1998; Trenberth 1998; Small and Kurc 2003), which may play a substantial role in the development of extreme droughts in North America (Saini et al. 2016) and temperature anomalies during heat waves, as noted over western Europe (Stefanon et al. 2013).

Large-scale patterns of weather conducive to heat waves can be affected by variations in sea surface temperatures (SSTs) in the world oceanic basins (Namias 1982; Lyon and Dole 1995) and Arctic sea-ice concentration (Watanabe et al. 2013). For example, McKinnon et al. (2016) have showed that significant predictability can be derived from midlatitude Pacific SSTs and antecedent rainfall, at 50-day lead for heat waves developping over the eastern US during summer. At inter-annual time-scales, La Niña events in the tropical eastern Pacific are conducive to dry conditions in the southwest US (Schubert et al. 2004a,b; Seager et al. 2005) that may lead to increased heat conditions. Eastern North America climate is also subject to the influence from the summer North Atlantic Oscillation (NAO) (Folland et al. 2009), the northerly-shifted counterpart of the winter NAO (Barnston and Livesey 1987; Hurrell and van Loon 1997; Hurrell and Folland 2002; Hurrell et al. 2003). It is a principal mode of climate variability in the North Atlantic-European summer that shows also significant correlations with climate in northeast North America where higher-than-average temperatures are related to positive phases of the summer NAO (Folland et al. 2009).

87 Folland et al. (2009) also evidenced partial relationships such that when the AMV is in its warm  
88 phase, the summer NAO tends to be in its negative phase. In their recent review Grotjahn et al.  
89 (2016) found that the influence from low frequency variability associated with ENSO and the NAO  
90 on warm episodes over North America are simulated with useful fidelity by global climate models.  
91 At multi-decadal time-scales, North American climate is influenced by the AMV (Enfield et al.  
92 2001; Sutton and Hodson 2005; Knight et al. 2006; Ting et al. 2009, 2011) but also the Pacific  
93 Decadal Oscillation (PDO) in boreal winter (Kenyon and Hegerl 2008). During summer, rela-  
94 tionships between weather patterns related to quasi-permanent ridges conducive to heat waves  
95 over North America and multi-decadal variability in the North Atlantic basin have been examined  
96 (Knight et al. 2006) but are not yet fully documented. Because the AMV is potentially predictable  
97 (Yang et al. 2013; Hermanson et al. 2014), summer climate in Europe and America might also be  
98 predictable on decadal time-scales (Kirtman et al. 2013; Seager and Ting 2017), thus motivating  
99 further investigation of potential linkages between recurrent heat wave-conducive weather patterns  
100 and North Atlantic SST fluctuations.

101 Heat waves are commonly seen as the result of subseasonal atmospheric variability (Teng et al.  
102 2013) and are generally associated with large scale meteorological patterns which are well resolved  
103 by global models (Grotjahn et al. 2016). Thus, our understanding of the underlying atmospheric  
104 dynamics at subseasonal time-scales and how these interact with large-scale climate modes of vari-  
105 ability is crucial to improve their prediction. This study diagnoses surface temperature variability  
106 during Jun-Sep (JJAS) over North America through a clustering of daily continental maximum  
107 temperature (Tmax) observed over the last 30 years, as well as simulated by historical and forced  
108 multi-decadal AGCM experiments in order to identify potential controls from the North Atlantic  
109 and specifically the AMV. The method and modeling experiments are presented in more detail  
110 in the next section. Results from the cluster analysis are then discussed in section 3 alongside

111 associated atmospheric circulation anomalies and large-scale teleconnections. In section 4, forced  
112 AGCM experiments are used to demonstrate the influence of the AMV on heat waves over the US.  
113 Discussion and conclusions are presented in section 5.

## 114 **2. Data and Methods**

### 115 *a. Atmospheric and land surface data*

116 1980-2009 daily atmospheric fields from NCEP-DOE II reanalysis (NCEP2), produced by the  
117 National Centers for Environmental Prediction (NCEP) and the US Department Of Energy (DOE),  
118 at  $2.5^{\circ} \times 2.5^{\circ}$  horizontal resolution (Kanamitsu et al. 2002), are used for model validation.

119 The relationships between each regime obtained from the clustering presented in the next section  
120 and sea surface conditions is assessed using the NOAA Extended Reconstructed SST version 3b  
121 (ERSST) with daily values at a quarter of a degree aggregated for JJAS seasons from 1980 to 2009.

### 122 *b. Modeling experiments*

123 The ECHAM5 AGCM used in this study is a spectral model with a triangular truncation at  
124 wavenumber 42 (T42) and 19 unevenly spaced hybrid sigma-pressure vertical layers (Simmons  
125 and Burridge 1981). A complete description of the model can be found in Roeckner (2003).

126 ECHAM5 is forced with prescribed historical global ERSSTs for the 1930-2013 period (ECHAM5  
127 GOGA). Prescribed sea ice concentrations are derived from the observational surface boundary  
128 forcing dataset for uncoupled simulations with the Community Atmosphere Model based on Hur-  
129 rell et al. (2008) that is a merged product of the monthly mean Hadley Centre sea ice and SST  
130 dataset version 1 (HadISST1, Rayner et al. (2003)) and version 2 of the NOAA weekly optimum  
131 interpolation (OI) SST analysis (Reynolds et al. 2002). Greenhouse gases concentrations are kept  
132 at the year 2000 value and there is no aerosol forcing. Sixteen ECHAM5 GOGA members are

133 generated using perturbed initial conditions to isolate the SST-driven signals by ensemble aver-  
134 aging which reduces internal atmospheric variability. Moreover, ECHAM5 has also been forced,  
135 over the same 84-year period, by observed SSTs in all oceanic basins except in the North Atlantic,  
136 where climatological SSTs computed over the 1930-2013 period (ECHAM5 CLM) and anoma-  
137 lous positive/negative SSTs mimicking the AMV phases (ECHAM5 AMV+/-) are prescribed to  
138 determine the impact of AMV SST patterns on continental warming. The AMV SST pattern is  
139 derived from linear regression of the standardized AMV index defined by Ting et al. (2009) onto  
140 North Atlantic SSTs for the period 1930 to 2013. The amplitude of regressed AMV SST anoma-  
141 lies is multiplied by 2.5 to obtain a robust response. Sixteen members are generated for CLM and  
142 AMV+/- using perturbed initial conditions.

### 143 *c. Dynamical clustering and significance testing*

144 Daily variability in maximum temperatures (Tmax) is examined through an objective classifi-  
145 cation based on the *k – means* clustering (Cheng and Wallace 2003; Michelangeli et al. 1995;  
146 Fereday et al. 2008) of continental daily Tmax anomalies (obtained by subtracting the mean an-  
147 nual cycle) from both NCEP2 and ECHAM5 modeling experiments over North America between  
148 0-60°N. To reduce the dimensionality of the problem and to ensure linear independence between  
149 input variables, an EOF analysis is first performed on the data correlation matrix and the first 11  
150 PCs explaining 69.6% of the variance for NCEP2 and 69.8% for ECHAM5 are retained for clus-  
151 tering analysis. The long-term trends are not removed from daily data, however, detrending does  
152 not lead to any difference in regime behavior (not shown), since the long-term trend contribution  
153 to Tmax variability over North America can be neglected at daily time-scale. The Euclidean dis-  
154 tance is then used to measure similarities between daily Tmax patterns and a given regime. To test  
155 the robustness of the regime partitions, 100 different partitions of daily Tmax anomaly patterns

156 are performed, each time with a different randomly drawn initialization (Michelangeli et al. 1995;  
157 Moron and Plaut 2003; Vigaud et al. 2012). The dependence of the final partition on the initial  
158 random draw is evaluated by comparing several final partitions for a given number of regimes  $k$ .  
159 The average similarity within the 100 sets of regimes is then measured by a classifiability index  
160 (Cheng and Wallace 2003), which evaluates the similarity within the 100 sets of regimes (i.e. its  
161 value would be exactly 1 if all the partitions were identical), and is compared to confidence limits  
162 from a red-noise test (applied to Markov-generated red-noise data) based on 100 samples of the  
163 same length. This operation provides 100 values of the classifiability index and is repeated for  
164  $k$  varying from 2 to 10. Fereday et al. (2008), who applied a similar  $k - means$  clustering but to  
165 mean sea level pressure over the North Atlantic-European sector, argue that this approach might  
166 not provide a suitable choice of the number of clusters. Nevertheless, the authors note that a com-  
167 promise as to be made and the 6-cluster partition we have chosen here using red-noise test (i.e.,  
168 the classifiability index discussed above) satisfy the condition that there are not too few clusters,  
169 so that the cluster centroids do not effectively span the space of data, but not so many so that the  
170 similarity between neighboring cluster centroids is not too great (Fereday et al. 2008).

171 All composites are statistically tested with Student's t-test and correlations with a resampling  
172 Monte-Carlo bootstrap test based on 100 random permutations (Livezey and Chen 1983).

### 173 **3. Maximum summer temperature variability over North America**

#### 174 *a. Recurring patterns*

175 The  $k - means$  classifiability index corresponding to the clustering of JJAS daily Tmax anoma-  
176 lies from a single member of ECHAM5 GOGA experiments (Fig. 1), here chosen randomly to  
177 illustrate the behavior in the model, exhibits the first index that is above red noise at  $k=6$  selected

178 for the analysis. Significance is not increased much for larger partitions as indicated by the respec-  
179 tive spread and median values, while no significance is found for  $k=8$ . Tmax anomalies are shown  
180 in Figure 2a to f for each regime. For validation purposes, these patterns are compared to those  
181 obtained from a similar clustering applied to NCEP2 reanalysis (Fig. 2g-l). Spatial pattern corre-  
182 lations between ECHAM5 and NCEP2 patterns for regime 1 to 6 are 0.90, 0.56, 0.93, 0.66, 0.76  
183 and 0.91, when computed over the respective 1930-2013 and 1980-2009 periods. Correlations of  
184 similar magnitude were obtained for the common 1980-2009 period.

185 Most patterns capture alternating warming/cooling centers over the US with contrasting posi-  
186 tive/negative Tmax anomalies. For example, regime 5 is characterized by warming north of  $40^{\circ}\text{N}$   
187 and weak cooling in the northwest and southeast, while regime 6 shows maximum positive anoma-  
188 lies over the northeast US resembling the pattern from McKinnon et al. (2016), and strong negative  
189 anomalies in the northwest. By contrast, regime 2 consists of broad warming across the US.

190 Regime transitions, which are defined as the number of event transitions from one regime to  
191 another, are illustrated in Table 1. The highest counts are found along the diagonal suggesting  
192 the persistence of each regime at the daily time-scale. In particular, maximum probabilities for  
193 regimes 2 (67%) and 5 (64%) reflect their prevalence and persistence, while related warming over  
194 most of the US and the northeast respectively suggest links to heat waves. Significant transition  
195 probabilities compared to chance indicate that regime 6 is generally followed by regime 1, which  
196 preferentially precedes regimes 3 and 4, while regime 3 tends to be followed by regime 5, which is  
197 consistent with the southeastwards transit of positive/negative anomalies seen from Figure 2f, a, c  
198 and e for ECHAM5 (l, g, i and k for NCEP2). Other regimes (2 and 4) are relatively independent  
199 from one another. .

200 *b. Related atmospheric circulation anomalies*

201 Regimes 6, 1 and 3, which tend to happen in sequence, as well as regime 4, are characterized  
202 by ridge-trough anomalies in the midlatitudes shown in 200 hPa geopotential heights composites  
203 (Fig. 3l, g, i and j) that extend to the surface (Fig. 3f, a, c and d), suggesting relationships to  
204 propagating synoptic waves potentially associated with baroclinic instability. The locations of the  
205 ridge embedded in this wave train correspond with positive Tmax anomalies for each regime (Fig.  
206 2f, a, c and d) and their transition eastwards over the US from regime 6, 1, to 3 or 4 is concomitant  
207 with the shift of high pressure anomalies further inferring relationships to westerly waves.

208 Regimes 2 and 5 are related to positive geopotential anomalies at upper levels over America,  
209 Europe and Asia (Fig. 3h and k), with maximum over the US, suggesting possible correlated heat  
210 waves occurrences in these regions of the Northern Hemisphere. Upper-tropospheric patterns are  
211 larger than the typical wave number 6 synoptic scale wave pattern, and could thus be associated  
212 with teleconnections, as reflected by the persistence of both regimes and no significant pattern tran-  
213 sition (Table 1). Regime 2 also displays low pressure anomalies north of the northeast/northwest  
214 US at both surface and upper-tropospheric levels (Fig. 3b and h). Regime 5 is related to a circum-  
215 polar pattern of positive anomalies with highest values over America at both upper-tropospheric  
216 levels and surface, with simultaneous low pressure anomalies over the northwest US and central  
217 North Atlantic at upper-tropospheric level (Fig. 3e and k). These translate at surface in a dipole  
218 pattern of high/low pressure anomalies in the southern/northern parts of the North Atlantic (Fig.  
219 3e) that resembles the positive phase of the summer NAO related to above average temperatures  
220 in northern Europe and northeast North America (Folland et al. 2009).

221 *c. Year-to-year variability and teleconnections to large-scale SSTs*

222 To determine the year-to-year variability of Tmax over the US and potential links to SSTs,  
223 NCEP2 and ECHAM5 ensemble mean JJAS Tmax anomalies are averaged for North America be-  
224 tween 21-55°N and plotted in Figure 4 alongside the annual AMV index, defined as the detrended  
225 SSTs averaged over [0°N-65°N;0-80°W]. Tmax anomalies are also reconstructed from the yearly  
226 frequencies of each regime, that are multiplied by associated Tmax anomalies and averaged spa-  
227 tially over the same North American domain, for each Jun-Sep season within the 1980-2009 and  
228 1930-2013 periods for NCEP2 and ECHAM5 ensemble mean, respectively. Spatially averaged  
229 Tmax anomalies are significantly correlated with those reconstructed from regime frequencies  
230 and mean Tmax anomalies in NCEP2 (0.88). Similarly, ECHAM5 ensemble mean Tmax anoma-  
231 lies are significantly related to reconstructed anomalies when averaged across ECHAM5 members  
232 (0.96), further indicating that Tmax variability is well represented by thermal regimes. In addi-  
233 tion, the five warmest seasons identified from NCEP2 and ECHAM5 JJAS Tmax indices (Fig. 4)  
234 generally coincide with less frequent regimes 1 and 3 but increased occurrences of regimes 2 and  
235 5 episodes, the opposite being true for coolest years, while relationships are less clear for other  
236 regimes (not shown).

237 Tmax anomalies are significantly correlated with the AMV for both NCEP2 (0.35) and  
238 ECHAM5 (0.44). For ECHAM5, correlations are less consistent before (0.23) than after (0.58,  
239 99% level significant) 1960, which might also reflect the lesser reliability of SST data. Moreover,  
240 higher (lower) number of regime 2 (1, 3 and 5) occurrences in 1930-60 when the AMV is positive  
241 compared to 1966-96 when the AMV is negative (Table 2), further suggest AMV controls and  
242 agree with the relationship between positive AMV phases and warming in the US (Sutton and

243 Hodson 2005; Ting et al. 2009, 2011).

244

245 For each regime separately, correlation patterns between the number of occurrences of each ther-  
246 mal regime (with the long term climatological mean removed) and seasonal JJAS SST anomalies  
247 (Fig. 5) bear some similarities when computed from 1980-2009 NCEP2 and averaged across 1930-  
248 2013 ECHAM5 GOGA members, the latter exhibiting more spatially coherent patterns which  
249 could be attributed to the filtering of internal variability in the model when aggregating across  
250 ensemble members. Overall, regime frequencies are mainly influenced by El Niño/La Niña and  
251 Pacific extratropics, the Atlantic and the tropical western Pacific/Indian basins, and their combina-  
252 tion. Interestingly, the regimes (1, 3 and 4) associated with synoptic wave patterns exhibit opposite  
253 relationships in both the Pacific and Atlantic compared to regimes 2 and 5 potentially associated  
254 with teleconnections. Regimes 2 and 5 are related to La Niña and warm conditions in the Atlantic  
255 basin, consistent with warming in the US for La Niña episodes (Schubert et al. 2004a,b; Seager  
256 et al. 2005) and positive AMV phases (Ting et al. 2009, 2011). Moreover, both regimes are also  
257 associated with warming in the west Pacific midlatitudes, in a pattern similar to the Pacific Ex-  
258 treme Pattern (PEP) from McKinnon et al. (2016) that has skill in predicting summer heat waves  
259 in the northeast US over the last 30 years.

#### 260 **4. Impact of the North Atlantic in idealized ECHAM5 experiments**

261 Superimposing AMV+/- SST anomalies in ECHAM5 experiments modulates maximum tem-  
262 peratures over North America, in particular over the central and western US (Fig. 6c). For AMV+  
263 experiments, in addition to warm air advection towards the central US at surface levels (Fig. 6a),  
264 warmer SSTs in the tropical Atlantic increase convection there and in the Intra-American Seas or  
265 IAS (Fig. 6c), leading to upper-tropospheric warming that extends beyond the North American

266 land mass (Fig. 6d). Warming at upper levels increases static stability in turn inhibiting rising  
267 motions most particularly over the western US (Fig. 6c and d), where stronger ridging anomalies  
268 in the upper-troposphere translate into warmer conditions compared to AMV-.

269 To investigate further potential controls from the North Atlantic, the clustering presented  
270 in the previous section for ECHAM5 GOGA has been replicated for ECHAM5 CLM and  
271 AMV+/- experiments (see section 2c) by applying *k – means* to daily Tmax anomalies from  
272 their corresponding ensemble member forced with the same perturbed initial conditions as those  
273 used for the GOGA member clustered in section 3a. Maximum classifiability is obtained for all  
274 experiments for a 6-cluster partition (not shown) and minimal Euclidean distances to ECHAM5  
275 GOGA clusters (not shown) suggest close correspondances between the pattern of anomalies  
276 typical of each regime. For each ECHAM5 experiments (CLM and AMV+/-), daily Tmax  
277 patterns from each ensemble member are next classified as a single regime occurrence for which  
278 Euclidean distance is minimized across the respective ECHAM5 clusters, hence allowing a direct  
279 evaluation of subsequent regime sequences across each ensemble experiments (i.e., CLM and  
280 AMV+/-). The anomalies averaged across all ECHAM5 AMV+ and AMV- ensemble members  
281 (Fig. 7 left and middle panels) are identical in structure to those from ECHAM5 GOGA (Fig. 2),  
282 only the magnitude of anomalies differs across experiments. Differences between mean Tmax  
283 patterns for ECHAM5 AMV+ and AMV- (Fig. 7 right panels) indicate that, for all regimes,  
284 warmer/cooler conditions imposed in the North Atlantic result in warmer/cooler anomalies most  
285 pronounced over the central and western US and western Canada, where highest differences for  
286 regimes 2 and 5 further suggest increased heat waves conditions for warm phases of the AMV.

287  
288 The proportions in the frequencies of occurrences of each regime are similar between NCEP2  
289 and when averaged across ECHAM5 GOGA ensemble members (Fig. 8a). The contrasting 30-

290 and 84-year periods pertaining to ECHAM5 GOGA and NCEP2 does not account much for the  
291 differences in regime frequencies as indicated by comparable ECHAM5 GOGA counts for the  
292 1980-2009 period (not shown); nevertheless, ECHAM5 GOGA displays more occurrences of  
293 regime 2 and 6 but less for the other regimes compared to NCEP2. A similar count to Figure  
294 8a is shown in Figure 8b across ECHAM5 CLM and AMV+/- sixteen members over the 1930-  
295 2013 period. The proportion of occurrences in all forced experiments are on average similar to  
296 ECHAM5 GOGA (Fig. 8a) and the spread amongst ensemble members is small compared to the  
297 mean frequencies. The differences between the regime frequencies averaged across ECHAM5  
298 CLM and GOGA ensemble members (Fig. 8c) show a significant increase (reduction) in the fre-  
299 quency of regimes 1, 2, 3 and 4 (5 and 6) in ECHAM5 CLM members compared to those from  
300 ECHAM5 GOGA. Increases in regimes 1, 2 and 3 frequencies are consistent with their greater  
301 relationships to ENSO than with the Atlantic basin (Fig. 5a, c and d), however modulations of  
302 regimes 4 and 6 frequencies are less easy to explain. While modulations for most regimes are be-  
303 low 20%, a reduction of up to 60% of regime 5 occurrences suggests that removing all variability  
304 except the seasonal cycle in the North Atlantic directly inhibits its development, which indicates  
305 primary influences from the Atlantic basin for that mode (Fig. 5e) and agrees with atmospheric  
306 circulation anomalies at surface resembling the positive summer NAO, itself partly related to the  
307 AMV (Folland et al. 2009). It emphasizes that interannual and higher variability in the basin exert  
308 controls on conditions favorable to the development of heat waves over North America.

309 Differences in yearly continental Tmax anomalies across ECHAM5 experiments when spatially  
310 averaged between 21-55°N are significantly correlated to those reconstructed from the frequencies  
311 and average Tmax anomalies of each regime (0.93, 0.95 and 0.94 for CLM minus GOGA, and  
312 AMV+/- minus CLM respectively), thus suggesting that Tmax differences over the US across  
313 ECHAM5 experiments are well represented by changes in thermal regimes and their frequencies.

314 Imposing AMV+/- anomalies in the North Atlantic increases/decreases the frequencies of  
315 regime 2 compared to ECHAM5 CLM (Fig. 8d), which is favored/inhibited with warming/cooling  
316 conditions in the North Atlantic (Fig. 5b-h). On average, AMV+ members have also more (less)  
317 frequent regime 4 (3, 5 and 6), while those for AMV- have less (more) frequent regime 1 (6).  
318 However, these differences remain small compared to those between ECHAM5 GOGA and CLM  
319 (Fig. 8c) and suggest that warmer SSTs in the North Atlantic act to increase anomalous warming  
320 in the central and western US across all regimes (Fig. 7), and influence their frequencies but less  
321 significantly. Regime 5 is inhibited in all forced ECHAM5 CLM and AMV+/- experiments, indi-  
322 cating that Tmax variability over the US is significantly influenced by the North Atlantic, however,  
323 the AMV contribution is not as strong as those from all time-scales beyond the seasonal cycle.

## 324 **5. Discussions and conclusions**

325 This study aimed at examining recurrent thermal regimes conducive to warming over North  
326 America during summer in order to identify how these are related to large-scale modes of climate  
327 variability, in particular the Atlantic Multi-decadal Variability (AMV). To this end, a dynamical  
328 clustering approach (*k – means*) was applied to ECHAM5 simulated daily Tmax in GOGA-like  
329 multidecadal experiments based on prescribed historical ERSSTs from 1930 to 2013, but also  
330 for validation purposes to NCEP2 reanalysis (1980-2009). This analysis allowed to identify six  
331 thermal regimes associated with significant Tmax anomalies over North America. Four regimes  
332 (1, 3, 4 and 6) are associated with a synoptic wave pattern propagating eastwards in the mid-  
333 latitudes, embedded ridging anomalies translating into maximum warming transiting along. Two  
334 other regimes, characterized by anomalous ridging over America, Europe and Asia, resemble more  
335 planetary waves potentially associated with teleconnections and are related to warming over the

336 whole of North America (regime 2) and the northeast US (regime 5), with potentially correlated  
337 heat waves in Europe and Asia.

338 At interannual time-scales, warmest/coolest years systematically coincide, as expected in both  
339 NCEP2 and ECHAM5, with increased/reduced occurrences of regimes 2 and 5, whose frequencies  
340 are increased for combined La Niña conditions in the Pacific and warming in the Atlantic, but  
341 also in the Pacific midlatitudes resembling the Pacific Extreme Pattern (McKinnon et al. 2016),  
342 consistent with the relationships of both basins to warmer conditions in North America (Schubert  
343 et al. 2004a,b; Seager et al. 2005; Ting et al. 2009, 2011; McKinnon et al. 2016). By contrast,  
344 the other regimes with stronger relationships to westerly waves are associated with opposite SST  
345 patterns in both basins. In particular, El Niño-like conditions tend to promote regimes 1, 3 and  
346 4, which tend to occur in sequence with regime 6. The latter is related to cooling in the tropical  
347 Pacific, thus warm ENSO conditions will tend to suppress regime 6 and could, in turn, alter  
348 regime sequences at subseasonal time-scales.

349  
350 Suppressing all variability beyond the seasonal cycle in the North Atlantic in ECHAM5 inhibits  
351 the frequency of regime 5 favorable to warming over the northeast US, in agreement with its  
352 primary relationships to Atlantic SSTs and surface circulation anomalies resembling the positive  
353 summer NAO partly related to the AMV (Folland et al. 2009). Superimposing positive/negative  
354 SST anomalies mimicking the AMV in the North Atlantic (ECHAM5 AMV+/-) translate in  
355 exacerbated/reduced warm conditions over the US observed across all regimes. Warmer SSTs in  
356 the tropical Atlantic for ECHAM5 AMV+ experiments increase convection locally, but also in  
357 the IAS, and lead to upper-tropospheric warming stretching over the North American land mass,  
358 which in turn increases static stability and suppresses rising motions most particularly over the  
359 western US, where warmer conditions prevail compared to AMV-. Positive/negative AMV SST

360 anomalies influence regime frequencies but less significantly compared to the magnitude of their  
361 associated Tmax anomalies, and thus systematically increase/decrease anomalous warming in the  
362 central and western US across all regimes, consistent with drought conditions and enhanced heat  
363 waves over North America during positive AMV phases (Mo et al. 2009; Schubert et al. 2009).  
364 Such controls from the North Atlantic contrast with the rather limited remote forcing from ENSO  
365 and the PDO on summer extreme temperatures events due to the relative inactivity and spatial  
366 extent of these climate modes during the warm season (Grotjahn et al. 2016). Despite different  
367 underlying mechanisms, AMV controls on ridging anomalies over North America resemble the  
368 impact of increasing greenhouse gases concentrations leading to upward trends in heat waves  
369 frequency and persistence in future projections through the intensification of a similar blocking  
370 ridge pattern (Meehl and Tebaldi 2004; Lau and Nath 2012).

371

372 The results presented here are based on coarse spatial resolution Tmax data suggesting that a  
373 similar set of regimes could be identified and used as a diagnostic of GCM forecast products. In  
374 this respect, this analysis provides a useful framework for heat wave predictability with dynamical  
375 evidence for significant relationships to thermal regimes reproducible in AGCM ensembles. The  
376 fact that some of the hottest episodes developed with recurrent thermal regimes over North Amer-  
377 ica, with potentials for correlated heat waves in Asia and Europe, is a direct motivation to examine  
378 their predictability in state-of-the-art forecast systems and benefit ongoing prediction efforts.

379 *Acknowledgments.* The authors are grateful to the reviewers whose insightful comments helped  
380 improve the manuscript, and would like to acknowledge the financial support from the NOAA  
381 Modeling, Analysis, Predictions and Projections (MAPP) Program NA14OAR4310223 grant led

382 by M. Ting at LDEO. Calculations were performed using IRI resources and the IRI Data Library  
383 (<http://iridl.ldeo.columbia.edu>) was used to access NCEP-DOE II reanalysis and NOAA ERSST.

## 384 **References**

385 Barnston, A., and R. Livesey, 1987: Classification, seasonality and persistence of low-frequency  
386 atmospheric circulation patterns. *Mon. Wea. Rev.*, **115**, 1083–1126.

387 Betts, A., and J. Ball, 1998: FIFE surface climate and site-averaged dataset 1987–1989. *J. Atmos.*  
388 *Sci.*, **55**, 1091–1108.

389 Brown, S. J., J. Caesar, and C. A. T. Ferro, 2008: Global changes in extreme daily temperature  
390 since 1950. *Geophys. Res.*, **113** (D05115), doi:10.1029/2006JD008091.

391 Cheng, X., and J. Wallace, 2003: Regime analysis of the Northern Hemisphere winter-time 500  
392 hPa height field: spatial patterns. *J Atmos Sci*, **50**, 2674–2696.

393 Christidis, N., P. A. Stott, S. Brown, G. C. Hegerl, and J. Caesar, 2005: Detection of changes  
394 in temperature extremes during the second half of the 20th century. *Geophys. Res. Lett.*,  
395 **32** (L20716), doi:10.1029/2005GL023885.

396 Coumou, D., and A. Robinson, 2013: Historic and future increase in the global land area affected  
397 by monthly heat extremes. *Clim. Change*, **118**, 771–82.

398 Eltahir, E., 1998: A soil moisture-rainfall feedback mechanism: 1. Theory and observations. *Water*  
399 *Resour. Res.*, **34**, 765–776.

400 Enfield, D., A. Mestas-Nunez, and P. Trimble, 2001: The Atlantic multidecadal oscillation and its  
401 relation to rainfall and river flows in the continental U.S. *Geophys. Res. Lett.*, **28**, 2077–2080.

402 Fereday, D., J. Knight, A. Scaife, and C. Folland, 2008: Cluster analysis of North Atlantic-  
403 European circulation types and links with tropical Pacific sea surface temperatures. *J. Clim.*,  
404 **21**, 3687–3703, doi:10.1175/2007JCLI1875.1.

405 Field, C. B., V. Barros, T. F. Stocker, and Q. Dahe, 2012: *Managing the Risks of Extreme Events*  
406 *and Disasters to Advance Climate Change Adaptation*. Cambridge University Press, 582pp pp.

407 Folland, C., J. Knight, H. Linderholm, D. Fereday, S. Ineson, and J. Hurrell, 2009: The summer  
408 North Atlantic Oscillation: Past, present, and future. *J. Clim.*, **22**, 1082–1103.

409 Grotjahn, R., and Coauthors, 2016: North American extreme temperature events and related large  
410 scale meteorological patterns: a review of statistical methods, dynamics, modeling, and trends.  
411 *Clim. Dyn.*, **46**, 1151–1184.

412 Hermanson, L., R. Eade, N. Robinson, N. Dunstone, M. Andrews, J. Knight, A. Scaife, and  
413 D. Smith, 2014: Forecast cooling of the Atlantic subpolar gyre and associated impacts. *Geo-*  
414 *phys. Res. Lett.*, **41** (14), 5167–5174.

415 Hurrell, J., and C. Folland, 2002: *A change in the summer circulation over the North Atlantic*,  
416 Vol. 25. International CLIVAR Project Office, Southampton, United Kingdom, 52-54 pp.

417 Hurrell, J., Y. Kushnir, G. Ottersen, and M. Visbeck, 2003: *An overview of the North Atlantic*  
418 *Oscillation. The North Atlantic Oscillation: Climatic Significance and Environmental Impact*,  
419 Vol. 134. Amer. Geophys. Union, 1-35 pp.

420 Hurrell, J., and H. van Loon, 1997: Decadal variations in climate associated with the North At-  
421 lantic Oscillation. *Climat. Change*, **36**, 301–326.

422 Hurrell, J. W., J. Hack, D. Shea, J. Caron, and J. Rosinski, 2008: A new sea surface temperature  
423 and sea ice boundary dataset for the Community Atmosphere Model. *J. Clim.*, **21**, 5145–5153.

- 424 Kanamitsu, M., W. Ebisuzaki, J. Woollen, S.-K. Yang, J. Hnilo, M. Fiorino, and G. L. Potter, 2002:  
425 NCEP-DOE AMIP-2 Reanalysis (R-2). *Bul. of the Atmos. Met. Soc.*, **Nov.**, 1631–1643.
- 426 Kenyon, J., and G. C. Hegerl, 2008: Influence of modes of climate variability on global tempera-  
427 ture extremes. *J. Clim.*, **21**, 3872–3889.
- 428 Kirtman, B., D. Anderson, G. Brunet, I. S. Kang, A. A. Scaife, and D. M. Smith, 2013: *Predictions*  
429 *from weeks to decades*. Springer, 205-235 pp.
- 430 Knight, J., C. Folland, and A. Scaife, 2006: Climate impacts of the Atlantic Multidecadal Oscilla-  
431 tion. *Geophys. Res. Lett.*, **33 (L17706)**, doi:10.1029/2006GL026242.
- 432 Lau, N.-C., and M. J. Nath, 2012: A model study of heat waves over North America: Meteorolog-  
433 ical aspects and projections for the twenty-first century. *J. Clim.*, **25**, 4761–4784.
- 434 Lau, W., and D. Waliser, 2011: *Intraseasonal Variability of the Atmosphere-Ocean Climate Sys-*  
435 *tem*. Springer, Berlin, Heidelberg, 613 pp.
- 436 Livezey, R., and W. Chen, 1983: Statistical field significance and its determination by Monte Carlo  
437 techniques. *Mon. Yea. Rev.*, **111**, 46–59.
- 438 Lyon, B., and R. Dole, 1995: A diagnostic comparison of the 1980 and 1988 US summer heat  
439 wave-droughts. *J. Clim.*, **8**, 1658–1675.
- 440 Madden, R., and P. Julian, 1971: Detection of a 40-50 day oscillation in the zonal wind in the  
441 tropical pacific. *J. of Atm. Sci.*, **28**, 702–708.
- 442 McKinnon, K., A. Rhines, M. Tingly, and P. Huybers, 2016: Long-lead predictions of eastern  
443 united states hot days from pacific sea surface temperatures. *Nature Geosci.*, **9**, 389–394.

- 444 Meehl, G., and C. Tebaldi, 2004: More intense, more frequent, and longer lasting heat waves in  
445 the 21st century. *Science*, **305**, 994–997.
- 446 Michelangeli, P., R. Vautard, and B. Legras, 1995: Weather regime occurrence and quasi-  
447 stationarity. *J Atmos Sci*, **52**, 1237–1256.
- 448 Mo, K., J. Schemm, and S. You, 2009: Influence of ENSO and the Atlantic multidecadal oscilla-  
449 tion on drought over the United States. *J. Clim.*, **22**, 6716–6740.
- 450 Moron, V., and G. Plaut, 2003: The impact of El Niño-Southern Oscillation upon weather regimes  
451 over Europe and the North Atlantic during boreal winter. *Int. J. Climatol.*, **23**, 363–379.
- 452 Namias, J., 1982: Anatomy of great plains protracted heat waves (especially the 1980 US summer  
453 drought). *Mon. Wea. Rev.*, **110**, 824–838.
- 454 Peterson, T., and Coauthors, 2013: Monitoring and understanding changes in heat waves, cold  
455 waves, floods, and droughts in the United States. *Bull. Am. Soc.*, 821–834, doi:10.1175/  
456 BAMS-D-12-00066.1.
- 457 Rayner, N., D. Parker, E. Horton, C. Folland, L. Alexander, D. Rowell, E. Kent, and A. Kaplan,  
458 2003: Global analyses of sea surface temperature, sea ice, and night marine air temperature  
459 since the late nineteenth century. *J. Geophys. Res.*, **108**.
- 460 Reynolds, R. W., N. Rayner, T. Smith, D. Stokes, and W. Wang, 2002: An improved in situ and  
461 satellite SST analysis for climate. *J. Clim.*, **15**, 1609–1625.
- 462 Roeckner, E., 2003: The atmospheric general circulation model ECHAM5. Part I: Model descrip-  
463 tion. *Max Planck Institute for Meteorology*, **349**, 127pp.

464 Saini, R., G. Wang, and J. Pal, 2016: Role of soil moisture feedback in the development  
465 of extreme summer drought and flood in the United States. *J. Hydrometeorol.*, doi:10.1175/  
466 JHM-D-15-0168.1.

467 Schubert, S., M. Suarez, P. Pegion, R. Koster, and J. Bacmeister, 2004a: On the cause of the 1930s  
468 Dust Bowl. *Science*, **303**, 1855–1859.

469 Schubert, S., M. Suarez, P. Pegion, R. Koster, and J. Bacmeister, 2004b: Causes of long-term  
470 drought in the U.S. Great Plains. *J. Clim.*, **17**, 485–503.

471 Schubert, S., H. Wang, and M. Suarez, 2011: Warm seasonal subseasonal variability and climate  
472 extremes in the Northern Hemisphere: the role of stationary Rossby waves. *J. Clim.*, **24**, 4773–  
473 4792.

474 Schubert, S., and Coauthors, 2009: A U.S. CLIVAR project to assess and compare the responses of  
475 global climate models to drought-related SST forcing patterns: Overview and results. *J. Clim.*,  
476 **(22)**, 5251–5272.

477 Seager, R., Y. Kushnir, C. Herweijer, N. Naik, and J. Velez, 2005: Modeling of tropical forcing  
478 of persistent droughts and pluvials over western North America: 1856–2000. *J. Clim.*, **18 (19)**,  
479 4065–4088.

480 Seager, R., and M. Ting, 2017: Decadal drought variability over North America: Mechanisms and  
481 predictability. *Curr. Clim. Change*, doi:10.1007/s40641-017-0062-1.

482 Simmons, A., and D. Burridge, 1981: An energy and angular momentum conserving vertical finite  
483 difference scheme and hybrid vertical coordinates. *Mon. Wea. Rev.*, **109**, 758–766.

- 484 Small, E., and S. Kurc, 2003: Tight coupling between soil moisture and the surface radiation bud-  
485 get in semi-arid environments: Implications for land-atmosphere interactions. *Water Resour.*  
486 *Res.*, **39**, 1–14.
- 487 Stefanon, M., P. Drobinski, F. D’Andrea, C. Lebeaupin-Brossier, and S. Bastin, 2013: Soil  
488 moisture-temperature feedbacks at meso-scale during summer heat waves over Western Europe.  
489 *Clim. Dyn.*, **42**, doi:10.1007/s00382-013-1794-9.
- 490 Sutton, R., and D. Hodson, 2005: Atlantic Ocean forcing of North American and European sum-  
491 mer climate. *Science*, **309**, 115118.
- 492 Teng, H., G. Branstator, H. Wang, G. A. Meehl, and W. M. Washington, 2013: Probability of US  
493 heat waves affected by a subseasonal planetary wave pattern. *Nature Geosci.*, **6**, 1056–1061.
- 494 Ting, M., Y. Kushnir, and R. Seager, 2011: Robust features of Atlantic Multi-decadal Variability  
495 and its climate impacts. *Geophys. Res. Lett.*, **38**, doi:10.1029/2011GL048712.
- 496 Ting, M., Y. Kushnir, R. Seager, and C. Li, 2009: Forced and internal twentieth-century SST trends  
497 in the North Atlantic. *J. Clim.*, **22**, 1469–1481.
- 498 Trenberth, K., 1998: Atmospheric moisture recycling: Role of advection and local evaporation. *J.*  
499 *Clim.*, **12**, 1368–1381.
- 500 Vigaud, N., B. Pohl, and J. Cretat, 2012: Tropical-temperate interactions over southern Africa  
501 simulated by a regional climate model. *Clim Dyn*, doi:10.1007/s00382-012-1314-3.
- 502 Watanabe, M., H. Shiogama, a. M. Y. Imada, M. Ishii, and M. Kimoto, 2013: Event attribution of  
503 the august 2010 Russian heat wave. *SOLA*, **9**, 65–68.
- 504 Yang, X., and Coauthors, 2013: A predictable AMO-like pattern in the GFDL fully coupled en-  
505 semble initialization and decadal forecasting system. *J. Clim.*, **26**, 650–661.

506 **LIST OF TABLES**

507 **Table 1.** Contingency tables between the six daily Tmax classes from ECHAM5 GOGA.  
508 In parentheses are indicated the respective transition probabilities (in %) ob-  
509 tained by dividing separate class counts by the sum of the columns of each row.  
510 Stars (\*) indicate significance at 99.9% level using a  $\chi^2$  test. . . . . 25

511 **Table 2.** Mean total number of occurrences of the daily Tmax classes in ECHAM5  
512 GOGA experiments averaged over 16 ensemble members during the 1930-  
513 60/1966-96 historical AMV positive/negative phases alongside their differ-  
514 ences. Stars (\*) indicate significance at 95% significance level using a Student  
515 t-test. . . . . 26

516 TABLE 1. Contingency tables between the six daily Tmax classes from ECHAM5 GOGA. In parentheses are  
 517 indicated the respective transition probabilities (in %) obtained by dividing separate class counts by the sum of  
 518 the columns of each row. Stars (\*) indicate significance at 99.9% level using a  $\chi^2$  test.

<b>From \ To</b>	<b>Class 1</b>	<b>Class 2</b>	<b>Class 3</b>	<b>Class 4</b>	<b>Class 5</b>	<b>Class 6</b>
<b>Class 1</b>	635* (42)	95 (6)	403* (27)	317* (21)	29 (2)	25 (2)
<b>Class 2</b>	71 (4)	1309* (67)	68 (3)	118 (6)	196 (10)	205 (10)
<b>Class 3</b>	42 (3)	64 (5)	787* (56)	256 (18)	250* (18)	3 (0)
<b>Class 4</b>	182 (11)	150 (9)	79 (5)	924* (54)	105 (6)	258 (15)
<b>Class 5</b>	126 (6)	199 (11)	65 (3)	31 (2)	1250* (64)	272 (14)
<b>Class 6</b>	454* (26)	150 (8)	2 (0)	50 (3)	116 (7)	999* (56)

519 TABLE 2. Mean total number of occurrences of the daily Tmax classes in ECHAM5 GOGA experiments aver-  
 520 aged over 16 ensemble members during the 1930-60/1966-96 historical AMV positive/negative phases alongside  
 521 their differences. Stars (\*) indicate significance at 95% significance level using a Student t-test.

<b>ECHAM5 GOGA</b>	<b>Class 1</b>	<b>Class 2</b>	<b>Class 3</b>	<b>Class 4</b>	<b>Class 5</b>	<b>Class 6</b>
<b>1930-60 AMV+</b>	490	945	392	539	719	574
<b>1966-96 AMV-</b>	529	867	451	563	770	599
<b>AMV+ minus AMV-</b>	-39*	+78*	-59*	-24	-51*	-25

522 **LIST OF FIGURES**

523 **Fig. 1.** Classifiability index for 1930-2013 JJAS Tmax simulated by ECHAM5 GOGA over con-  
524 tinental North America as a function of the number of regimes  $k$  (boxes). The levels of  
525 significance at 95% (dashed line) are computed according to a first-order Markov process. . . . 28

526 **Fig. 2.** Mean Tmax anomalies (in  $^{\circ}\text{C}$ ) for each regime simulated by ECHAM5 GOGA (a to f) and  
527 from NCEP2 reanalysis (g to l) during JJAS over the 1930-2013 and 1980-2009 periods  
528 respectively. Only the grid-points for which anomalies are significant at 95% level using a  
529 Student t-test are displayed. . . . . 29

530 **Fig. 3.** Mean daily 850 hPa geopotentials (shadings in  $m$ , contours starting at and every  $\pm 5$ mb)  
531 with winds anomalies (vectors in  $m/s$ ) and 200 hPa geopotentials anomalies (shadings in  
532  $m$ , contours starting at and every  $\pm 10$ mb) for each Tmax regime simulated by ECHAM5  
533 GOGA (a to f and g to l) during JJAS over the 1930-2013 period. Only the grid-points for  
534 which anomalies are significant at 95% significance level are displayed (for vectors at least  
535 one component). . . . . 30

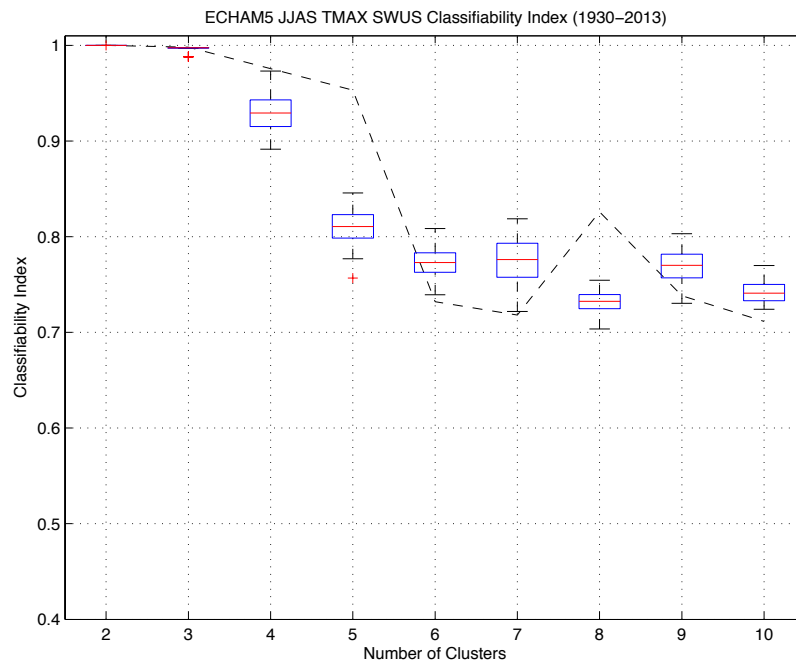
536 **Fig. 4.** Yearly JJAS Tmax anomalies (ECHAM5 GOGA ensemble mean in bars, NCEP2 plotted in  
537 blue) over North America between  $21-55^{\circ}\text{N}$  (in  $^{\circ}\text{C}$ ) together with the AMV index (green  
538 line). Tmax anomalies reconstructed from regime frequencies and average Tmax anomalies  
539 in NCEP2 are plotted in thick blue and those averaged across ECHAM5 GOGA ensemble  
540 members in thick black. . . . . 31

541 **Fig. 5.** Mean correlations (shadings) between each regime frequencies of occurrences averaged  
542 across ECHAM5 GOGA ensemble members and prescribed SSTs (a to f) for the 1930-  
543 2013 period. Similar correlations are presented between NCEP2 Tmax regime frequencies  
544 of occurrences and ERSSTs (g to l) during the 1980-2009 period. The black lines indicate  
545 correlations significant at 90% level of significance using Monte-Carlo simulations. . . . . 32

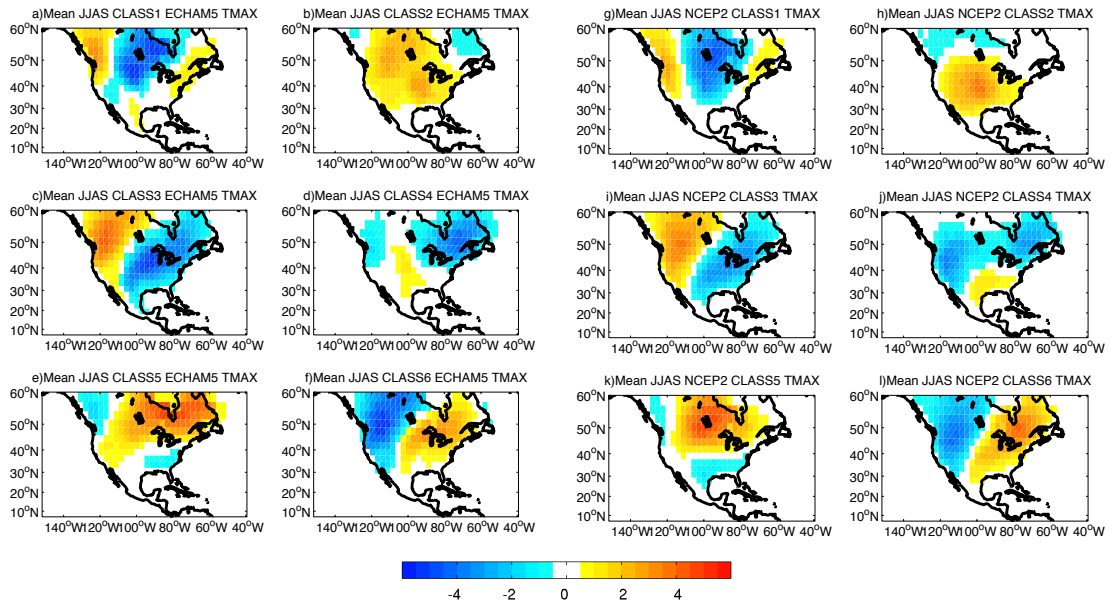
546 **Fig. 6.** Mean differences in (a) 850 hPa geopotentials (shadings in  $m$ , contours starting at and every  
547  $\pm 5 m$ ) and winds (vectors in  $m/s$ ), (b) 200 hPa geopotentials (shadings in  $m$ , contours  
548 starting at and every  $\pm 10 m$ ), (c) Tmax (shadings) and 500 hPa vertical velocities (contours  
549 starting at and every  $\pm 0.004 Pa/s$ ), and (d) tropospheric temperatures (shading in  $Celsius$ )  
550 and vertical velocities (contours starting at and every  $\pm 0.004 Pa/s$ ) between AMV+ and  
551 AMV- ECHAM5 ensemble mean during JJAS over the 1930-2013 period. Blue and red  
552 contours of vertical velocities correspond to rising and sinking motions, respectively, and the  
553 zero line is plotted in black. Only the grid-points for which differences are significant at 95%  
554 level of significance using Student t-test are displayed (for vectors at least one component). . . . 33

555 **Fig. 7.** Mean ECHAM5 AMV+ (left) and AMV- (center) Tmax anomalies for each class and their  
556 differences (right) averaged across all ensemble members over the 1930-2013 period (in  
557  $^{\circ}\text{C}$ ). Only the grid-points for which anomalies and differences are significant at 95% level  
558 of significance using Student t-test are displayed. . . . . 34

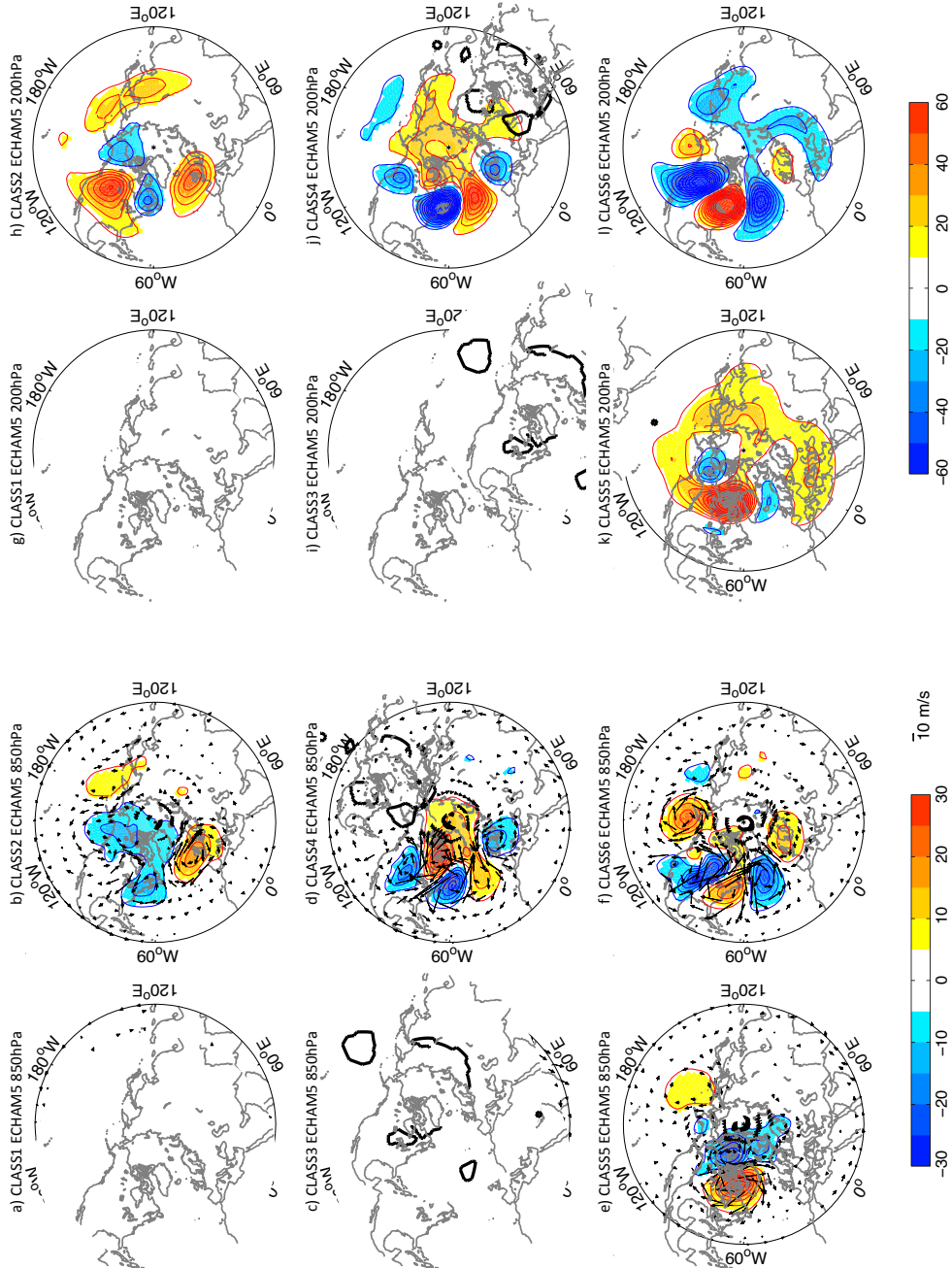
559 **Fig. 8.** Relative number of occurrences of Tmax classes in NCEP2 over the 1980-2009 period (blue)  
560 and averaged across ECHAM5 GOGA ensemble members over the 1980-2009 (orange) and  
561 1930-2013 (red) periods (a), together with these for ECHAM5 CLM and AMV+/- ensemble  
562 experiments (b) and differences between ECHAM5 CLM and GOGA (c) as well as AMV+/-  
563 and CLM (d) averaged across all ensemble members expressed as a percentage of total  
564 occurrences for each regime over the 1930-2013 period. Note that all differences in (c) are  
565 statistically significant at 90% level of significance using a Student t-test, while significant  
566 differences are indicated by a star (\*) in (d). . . . . 35



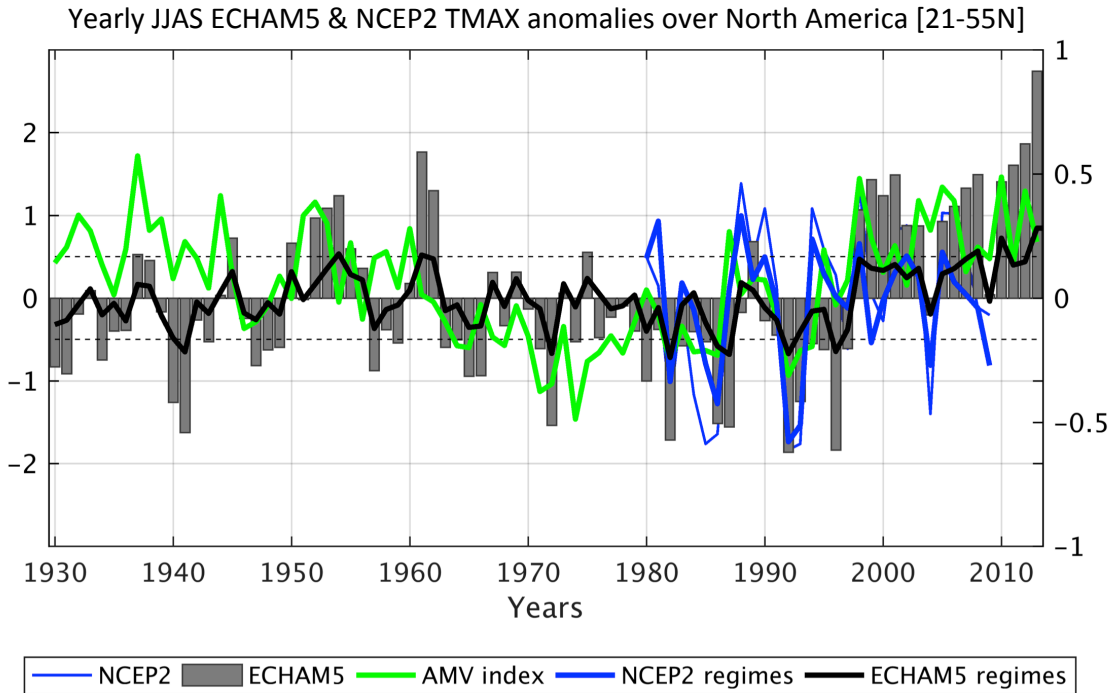
567 FIG. 1. Classifiability index for 1930-2013 JJAS Tmax simulated by ECHAM5 GOGA over continental North  
 568 America as a function of the number of regimes  $k$  (boxes). The levels of significance at 95% (dashed line) are  
 569 computed according to a first-order Markov process.



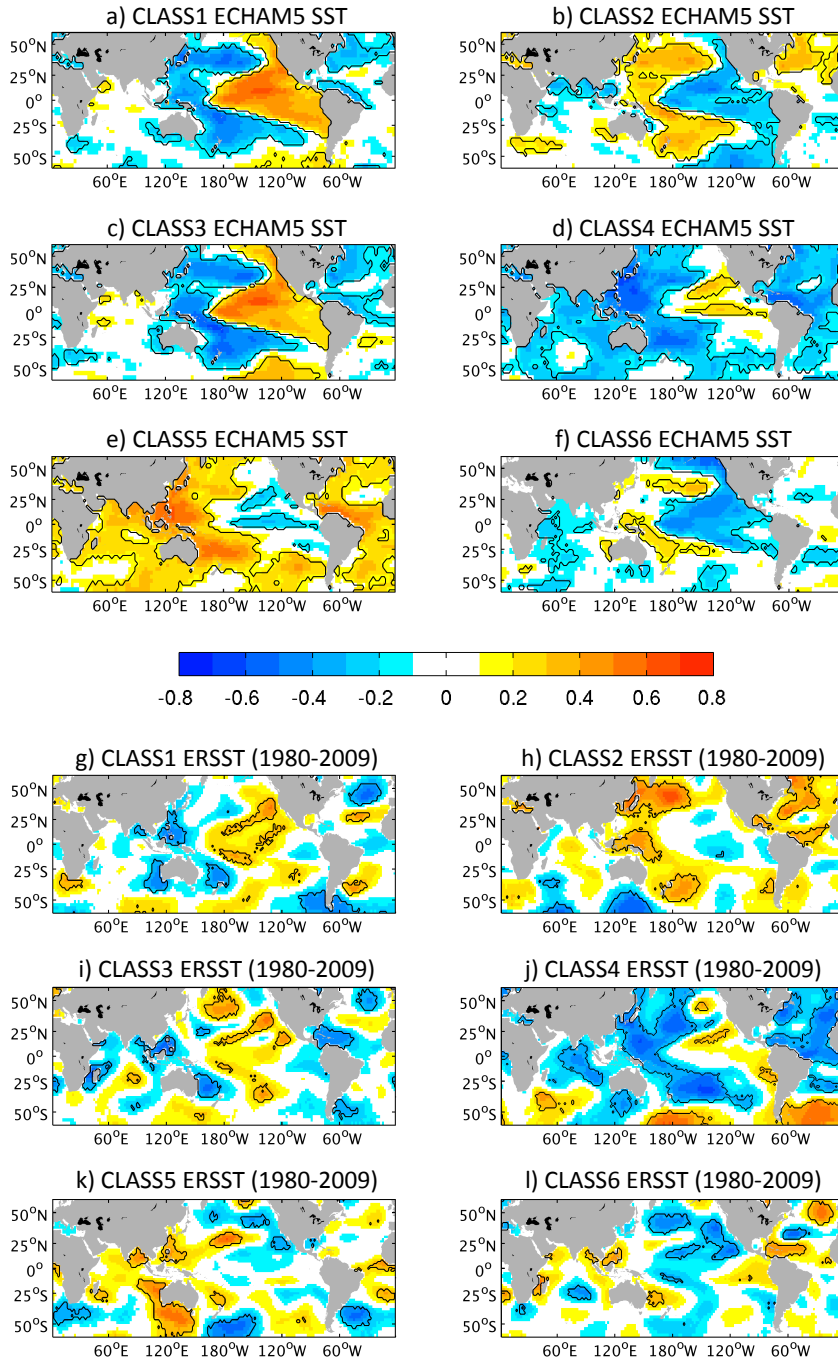
570 FIG. 2. Mean T<sub>max</sub> anomalies (in °C) for each regime simulated by ECHAM5 GOGA (a to f) and from  
 571 NCEP2 reanalysis (g to l) during JJAS over the 1930-2013 and 1980-2009 periods respectively. Only the grid-  
 572 points for which anomalies are significant at 95% level using a Student t-test are displayed.



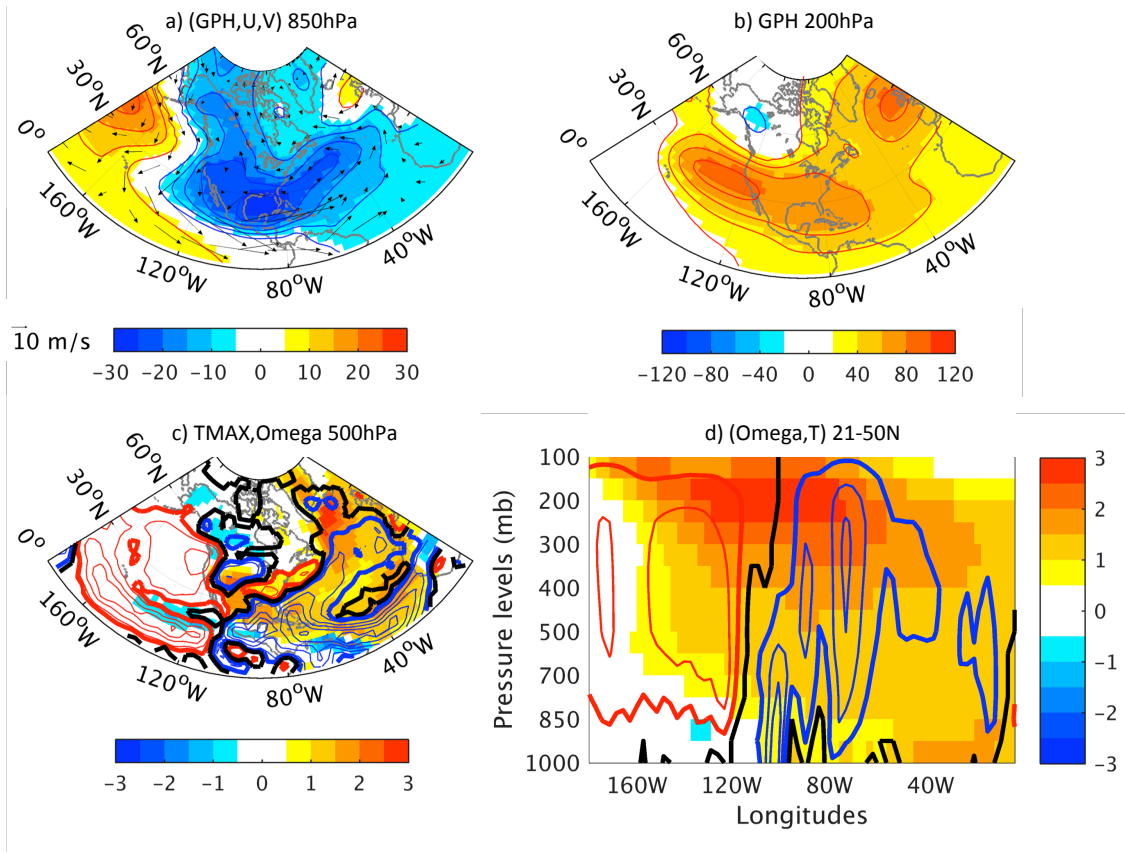
573 FIG. 3. Mean daily 850 hPa geopotentials (shadings in  $m$ , contours starting at and every  $\pm 5$ mb) with winds  
 574 anomalies (vectors in  $m/s$ ) and 200 hPa geopotentials anomalies (shadings in  $m$ , contours starting at and every  
 575  $\pm 10$ mb) for each Tmax regime simulated by ECHAM5 GOGA (a to f and g to l) during JJAS over the 1930-  
 576 2013 period. Only the grid-points for which anomalies are significant at 95% significance level are displayed  
 577 (for vectors at least one component).



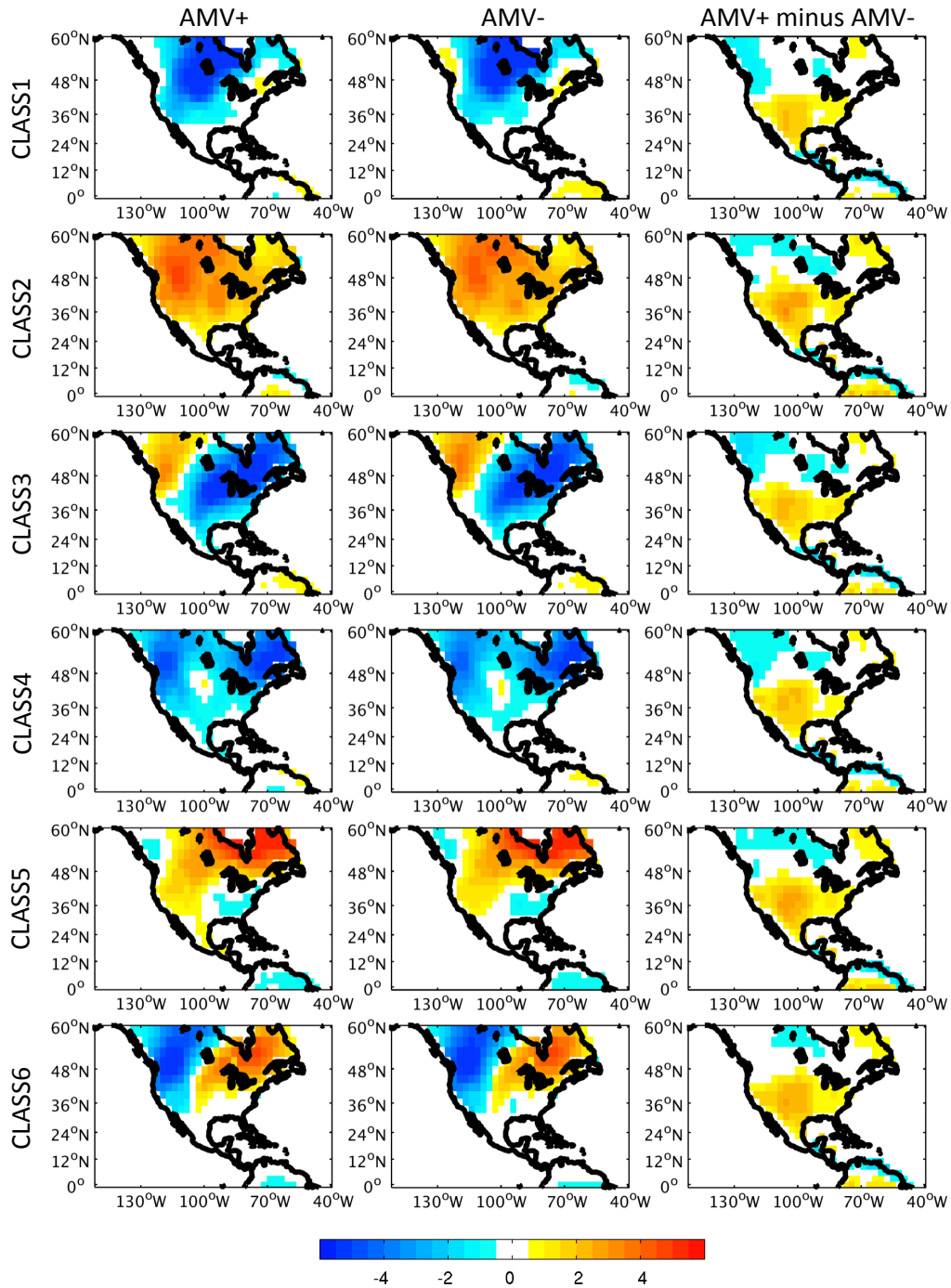
578 FIG. 4. Yearly JJAS Tmax anomalies (ECHAM5 GOGA ensemble mean in bars, NCEP2 plotted in blue)  
 579 over North America between 21-55°N (in °C) together with the AMV index (green line). Tmax anomalies  
 580 reconstructed from regime frequencies and average Tmax anomalies in NCEP2 are plotted in thick blue and  
 581 those averaged across ECHAM5 GOGA ensemble members in thick black.



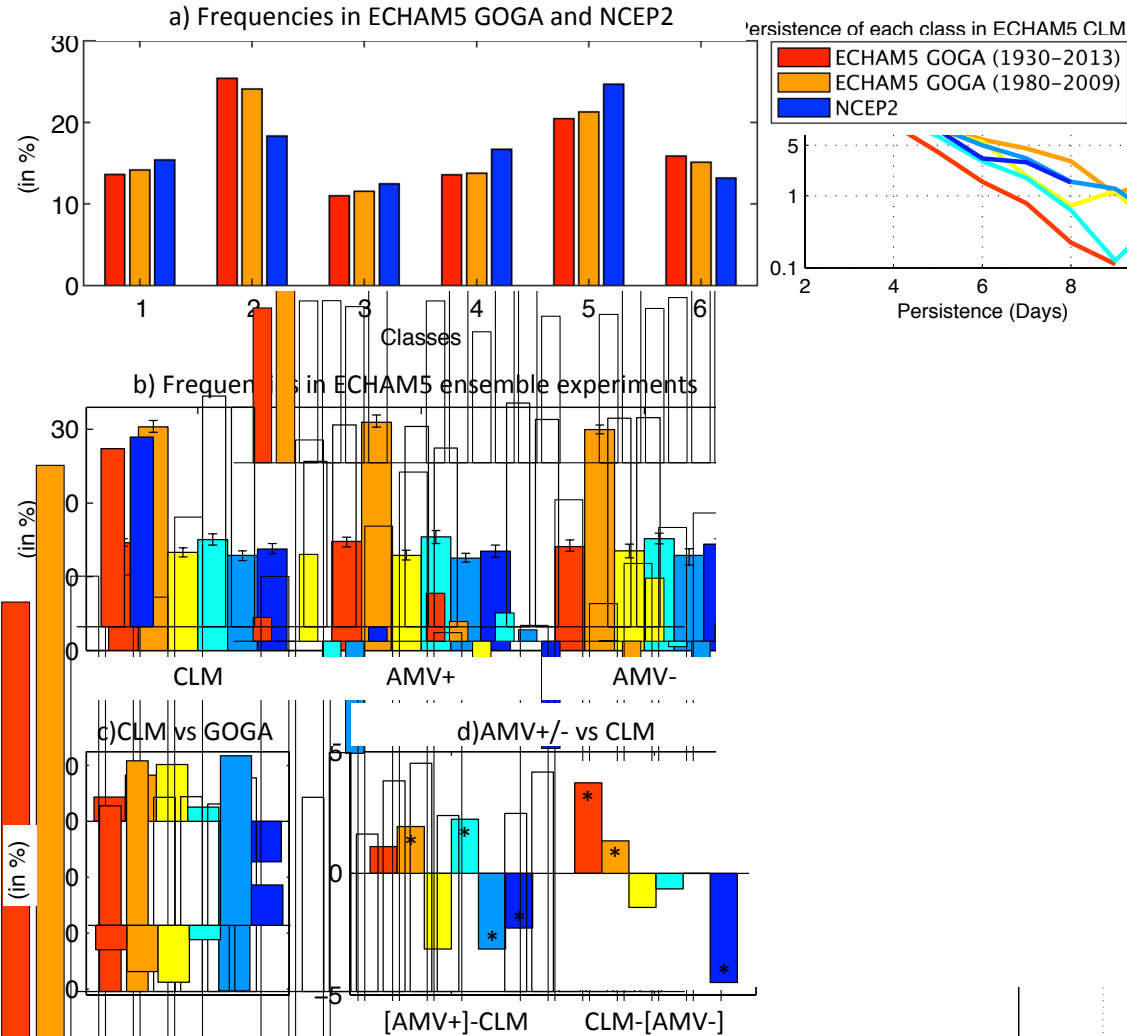
582 FIG. 5. Mean correlations (shadings) between each regime frequencies of occurrences averaged across  
 583 ECHAM5 GOGA ensemble members and prescribed SSTs (a to f) for the 1930-2013 period. Similar corre-  
 584 lations are presented between NCEP2 Tmax regime frequencies of occurrences and ERSSTs (g to l) during the  
 585 1980-2009 period. The black lines indicate correlations significant at 90% level of significance using Monte-  
 586 Carlo simulations.



587 FIG. 6. Mean differences in (a) 850 hPa geopotentials (shadings in  $m$ , contours starting at and every  $\pm 5$   
 588  $m$ ) and winds (vectors in  $m/s$ ), (b) 200 hPa geopotentials (shadings in  $m$ , contours starting at and every  $\pm 10$   
 589  $m$ ), (c) Tmax (shadings) and 500 hPa vertical velocities (contours starting at and every  $\pm 0.004 Pa/s$ ), and (d)  
 590 tropospheric temperatures (shading in  $Celsius$ ) and vertical velocities (contours starting at and every  $\pm 0.004$   
 591  $Pa/s$ ) between AMV+ and AMV- ECHAM5 ensemble mean during JJAS over the 1930-2013 period. Blue and  
 592 red contours of vertical velocities correspond to rising and sinking motions, respectively, and the zero line is  
 593 plotted in black. Only the grid-points for which differences are significant at 95% level of significance using  
 594 Student t-test are displayed (for vectors at least one component).



595 FIG. 7. Mean ECHAM5 AMV+ (left) and AMV- (center) Tmax anomalies for each class and their differences  
 596 (right) averaged across all ensemble members over the 1930-2013 period (in °C). Only the grid-points for which  
 597 anomalies and differences are significant at 95% level of significance using Student t-test are displayed.



598 FIG. 8. Relative number of occurrences of Tmax classes in NCEP2 over the 1980-2009 period (blue) and av-  
 599 eraged across ECHAM5 GOGA ensemble members over the 1980-2009 (orange) and 1930-2013 (red) periods  
 600 (a), together with these for ECHAM5 CLM and AMV+/- ensemble experiments (b) and differences between  
 601 ECHAM5 CLM and GOGA (c) as well as AMV+/- and CLM (d) averaged across all ensemble members ex-  
 602 pressed as a percentage of total occurrences for each regime over the 1930-2013 period. Note that all differences  
 603 in (c) are statistically significant at 90% level of significance using a Student t-test, while significant differences  
 604 are indicated by a star (\*) in (d).